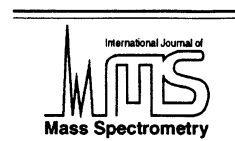




ELSEVIER

International Journal of Mass Spectrometry 195/196 (2000) 55–69



# Bimolecular ion-molecule collisions in real time: $\text{Co}^+(\text{}^3\text{F}_4) + n\text{-butane}$ and isobutane reactions

Emily L. Reichert, Sung Soo Yi, James C. Weisshaar\*

*Department of Chemistry, 1101 University Avenue, University of Wisconsin-Madison, Madison, WI 53706-1396, USA*

Received 28 April 1999; accepted 30 August 1999

## Abstract

A pulsed beam of  $\text{Co}^+(\text{}^3\text{F}_4)$  is crossed with a pulsed beam of  $n$ -butane or isobutane gas under single collision conditions at collision energies of 0.01 eV and 0.22 or 0.23 eV, respectively. After a variable time delay  $t_{\text{ext}} = 1\text{--}8 \mu\text{s}$ , a fast high voltage pulse extracts product ions and residual reactant ions into a field-free flight tube for mass analysis. Consistent with earlier work, we observe four product channels in the  $\text{Co}^+ + n\text{-butane}$  reaction: long-lived  $\text{CoC}_4\text{H}_{10}^+$  complexes and three elimination products,  $\text{CoC}_2\text{H}_4^+ + \text{C}_2\text{H}_6$ ,  $\text{CoC}_3\text{H}_6^+ + \text{CH}_4$ , and  $\text{CoC}_4\text{H}_8^+ + \text{H}_2$ . In the  $\text{Co}^+ + \text{isobutane}$  reaction, we detect long-lived  $\text{CoC}_4\text{H}_{10}^+$  complexes and two elimination products,  $\text{CoC}_3\text{H}_6^+ + \text{CH}_4$  and  $\text{CoC}_4\text{H}_8^+ + \text{H}_2$ . We discuss plausible mechanisms for these reactions, based on insights from our recent statistical modeling based on density functional theory (B3LYP) calculations for the related systems,  $\text{Ni}^+ + \text{propane}$ ,  $\text{Co}^+ + \text{propane}$ , and  $\text{Ni}^+ + n\text{-butane}$ . The postulated reaction pathways for  $\text{Co}^+ + n\text{-butane}$  and  $\text{Co}^+ + \text{isobutane}$  neatly explain the data from our experiment and a variety of others. From a combination of theory and experiments, a satisfyingly consistent picture of the reactions of late 3d-series metal cations with alkanes has emerged. (Int J Mass Spectrom 195/196 (2000) 55–69) © 2000 Elsevier Science B.V.

**Keywords:** Ion-molecule reactions; Time-of-flight mass spectrometry; Transition metal chemistry; Time-resolved bimolecular collisions; Crossed-beam technique; Gas-phase ion chemistry

## 1. Introduction

With the advent of density functional theory (DFT), detailed electronic structure calculations on systems of significant complexity are becoming feasible, allowing the comparison of theory and experiment in larger systems. One area which has recently benefited from this trend is the chemistry of gas phase transition metal cations with small alkanes [1]. A wealth of experimental data has appeared over some

two decades, but the postulated mechanisms have been somewhat speculative. Electronic structure calculations have only recently been brought to bear on these systems, complementing the extensive body of experimental work by providing new mechanistic insight. The results have been surprising and sometimes contradictory to mechanisms that had been previously assumed [2–5]. Recent studies of the reactions of  $\text{Fe}^+$  [5,6],  $\text{Co}^+$  [4,7], and  $\text{Ni}^+$  [2,3,8] with small alkanes using DFT in its B3LYP formulation [9] have found the lowest energy pathways to elimination to be highly concerted, involving fewer potential minima than the stepwise mechanisms long postulated for these reactions. Following insertion

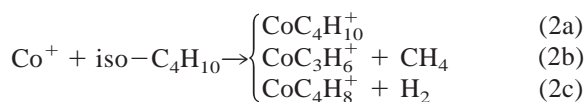
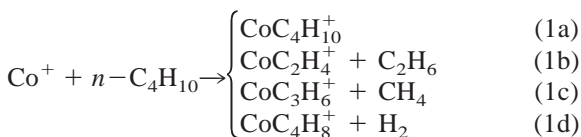
\* Corresponding author.

JCW dedicates this article to Bob Squires, who was always a warm, strong, brave human being and a good friend.

into the weakest CC or CH bond of the alkane, passage over a multicenter transition state (MCTS) stabilized by agostic interactions [10,11] is typically the rate-determining step en route to elimination of small alkanes or H<sub>2</sub>.

We have now completed studies of Ni<sup>+</sup> + propane [2], Ni<sup>+</sup> + *n*-butane [3], and Co<sup>+</sup> + propane [4], in which we report detailed comparisons of experimental data with the results of statistical rate modeling based on DFT (B3LYP) structures and energetics for key intermediates and transition states. Our crossed-beam experiment provides time-resolved branching fractions measured under carefully controlled reaction conditions, ideal for comparison with theory. We use time-of-flight mass spectrometry to monitor the decay of long-lived bimolecular complexes *in real time* following initiation of ion-molecule collisions at a sharp zero of time using an ionizing laser pulse. As explained by the modeling, angular momentum conservation plays a key role in the nonexponential decay of these complexes and in product branching [2–4].

Based on our modeling efforts, we have been able to construct a rather comprehensive picture of the mechanism of these reactions. Here we apply these mechanistic ideas to two more reactions, Co<sup>+</sup> + *n*-butane and Co<sup>+</sup> + isobutane. To our knowledge, no calculations have been performed on these systems, although the body of experimental work is extensive. Our experimental results for these systems complements earlier work on the same reactions by the Freiser and Ridge groups [12,13], who explored the collision-induced dissociation of product ions using Fourier transform mass spectrometry; by Armentrout and Beauchamp [14,15], who used isotopic labeling to infer mechanistic details, and by the Bowers group [16], who studied product kinetic energy release distributions (KERDs).



By applying concepts gleaned from the B3LYP calculations for Ni<sup>+</sup> + propane, Ni<sup>+</sup> + *n*-butane and Co<sup>+</sup> + propane, we postulate plausible lowest energy reaction pathways for the major elimination channels in the Co<sup>+</sup> + *n*-butane and Co<sup>+</sup> + isobutane reactions. Our predicted pathways are in good agreement with the data from our experiment and a variety of others [12,16,17]. Moreover, their success provides further evidence that a simple, consistent set of concepts can explain all reactions of Fe<sup>+</sup>, Co<sup>+</sup>, and Ni<sup>+</sup> with small alkanes.

## 2. Experimental section

### 2.1. Crossed-beam measurements

The crossed-beam apparatus and its usual operating parameters have been described previously [18,19]. In the source chamber, gas-phase cobalt atoms are produced in a laser ablation source [20,21] and seeded into an argon beam, which is skimmed, collimated, and stripped of ions before entering the reaction chamber. The Co/Ar beam meets a second, pulsed expansion of hydrocarbon gas at the center of the interaction region. The reaction begins with the arrival of an ionizing dye laser pulse at the center of this region, creating Co<sup>+</sup> cations in their ground electronic state. The Co<sup>+</sup> cations react with hydrocarbon molecules in field-free space via bimolecular ion-molecule collisions. After a suitable reaction delay, a high voltage pulse accelerates reactant and product ions toward a microchannel plate detector. The experiment runs in the single-collision regime.

A frequency-doubled dye laser beam (10 ns fwhm, 312 nm, <250 μJ/pulse) intersects the atomic beam and resonantly photoionizes Co by way of the  $y^4\text{G}_{7/2}^\circ \leftarrow a^4\text{F}_{9/2}$  transition at 32,028 cm<sup>-1</sup> [22]. Absorption of two such photons creates Co<sup>+</sup> exclusively in the ground spin-orbit level (<sup>3</sup>F<sub>4</sub>). The two-photon energy lies 491 cm<sup>-1</sup> above the ionization energy (IE) of

63,565  $\text{cm}^{-1}$  [23]. The nearest  $\text{Co}^+$  excited state is  $^3\text{F}_3$  at 951  $\text{cm}^{-1}$  above the IE. A log-log plot of  $\text{Co}^+$  ion yield versus laser pulse energy is linear with a slope of unity, consistent with a two-photon process whose first step is saturated. The metal ion velocity is that of the neutral beam,  $(5.8 \pm 0.5) \times 10^4$  cm/s [19].

The packet of  $\text{Co}^+$  (2000–7000 ions/shot) intersects the reagent beam in the extraction region of a Wiley-McLaren time-of-flight mass spectrometer [24]. Neat *n*-butane or isobutane gas (Matheson >99.9%) expands from a second 0.5 mm pulsed nozzle and is pseudoskimmed (i.e., not differentially pumped) by a set of homebuilt rectangular knife edges. The mean *n*-butane beam velocity measured with a fast ion gauge is  $(6.7 \pm 1.0) \times 10^4$  cm/s; the mean isobutane beam velocity is  $(7.0 \pm 1.0) \times 10^4$  cm/s. We see no evidence of heavier products that might indicate the presence of a significant fraction of dimers in either the *n*-butane or the isobutane beam. In addition, plots of product yield versus reagent backing pressure are linear from 20–120 Torr for both gases, indicating that single-collision conditions are obtained at 60 Torr and further, suggesting that the beams consist primarily of monomers. Based on the work of Fenn and co-workers [25], we estimate the internal temperature of both reagent gases to be  $\sim 50$  K.

By changing the angle between the  $\text{Co}^+$  and reagent beams, we can vary the collision energy in coarse steps. We have conducted experiments at two such geometries,  $20^\circ$  and  $145^\circ$ . The corresponding collision energies are  $0.01 \pm 0.01$  eV ( $0.2 \pm 0.2$  kcal/mol) and  $0.22 \pm 0.09$  eV ( $5.0 \pm 2.1$  kcal/mol) for *n*-butane, and  $0.01 \pm 0.01$  eV ( $0.2 \pm 0.2$  kcal/mol) and  $0.23 \pm 0.09$  eV ( $5.2 \pm 2.1$  kcal/mol) for isobutane. The estimated uncertainties reflect worst-case analyses accounting for uncertainties in the metal and hydrocarbon velocities, the small additional velocity imparted to the metal ions by space charge effects and the range of angles of intersection of the two velocity vectors.

The 10 ns laser pulse initiates ion-molecule collisions at a sharply defined starting time. After a variable delay time that allows collisions to occur,

reactant and product ions are extracted at time  $t_{\text{ext}}$  after the laser pulse into the time-of-flight mass spectrometer for analysis. We can obtain useful signals for extraction times in the range  $0.5 \mu\text{s} \leq t_{\text{ext}} \leq 8 \mu\text{s}$ . At  $t_{\text{ext}}$ , high-voltage pulses (1–1.5 kV) are applied to the ion extraction plates, accelerating reactant and product ions towards the detector. The voltage pulses rise to 90% of their plateau values in 20 ns; the analogous rise time of the electric field in the first extraction region is  $\sim 13$  ns. The mass resolution ( $m/\Delta m$ ) is  $>250$  for products near 100 u. Ions are detected with a microchannel plate detector (Galileo FTD-2003, Sturbridge, MA) operated at  $2 \times 10^7$  gain. The detector output current drops over the 50- $\Omega$  load on a LeCroy 9400 digital oscilloscope (LeCroy, Chestnut Ridge, NY) without further amplification. We estimate detector mass discrimination effects at less than 10% [26]. Since the detector dynamic range cannot simultaneously accommodate the  $\text{Co}^+$  ion signal and the much smaller product ion signals, a small set of electrodes mounted in the drift region is pulsed at the appropriate time to deflect  $\text{Co}^+$  ions away from the detector [19].

Under single-collision conditions, total product signal should rise linearly with  $\text{Co}^+$  number density, hydrocarbon number density, and  $t_{\text{ext}}$ , which we have experimentally verified. Moreover, the reaction should be insensitive to argon backing pressure. We have run the experiment at twice and half the normal argon backing pressure of 1.7 atm with  $t_{\text{ext}} = 8 \mu\text{s}$  and observe no changes in branching fractions or product yield relative to  $\text{Co}^+$  ion signal.

It is important to clearly distinguish two different time scales. The first is the experimental time window during which the  $\text{Co}^+$  and the *n*-butane or isobutane beams are “in contact” and collisions at a well defined energy may occur. This is the time between the ionizing laser pulse and the ion extraction pulse at  $t_{\text{ext}}$ . The second, which we simply call  $t$ , refers to the time elapsed since a long-lived complex was formed in a bimolecular collision. Because our experiment is firmly in the single-collision limit, to a good approximation we create collision complexes with a uniform distribution of initiation times over a time window of width  $t_{\text{ext}}$ . When we sample the fate of this collection

of complexes at a particular real experimental time after the ionizing laser pulse, as in a time-of-flight mass spectrum, we sample complexes that have evolved over a corresponding distribution of times  $t$  after the initiation of the collision. This is the range of times referred to in subsequent tables of time-dependent product branching fractions.

## 2.2. Analysis of metastable decay by retarding potential method

Under our controlled reaction conditions, the product mass spectra reveal long-lived collision complexes [Eqs. (1a) and (2a)]. Such complexes have survived extraction intact, because they arrive at the detector at the appropriate time for the adduct ion. These complexes are metastable. They have sufficient energy to fragment either to reactants or to exothermic elimination products. The time during which the complex is accelerated by the extraction fields is  $\sim 2 \mu\text{s}$  for the typical ion extraction energy of 1280 eV. For  $t_{\text{ext}} = 8 \mu\text{s}$ , complexes that survive  $t = 2\text{--}25 \mu\text{s}$  after they are formed may fragment in the field-free drift region of the mass spectrometer. Even longer-lived complexes will reach the detector intact.

Such metastable decay can be analyzed by applying a retarding potential in the flight tube between the extraction region and the detector, as described previously [18]. The retarding potential device alters arrival times in a mass-dependent fashion by first decelerating and then accelerating the ions back to their original drift velocity. In the examples presented below, we are able to distinguish long-lived complexes that survive the entire flight path intact and complexes that fragment in the first field-free region F1 (Fig. 2 of Ref. 18) before entering the retarding field. In previous studies of reactions with a larger proportion of the adduct, we have been able to identify fragments formed in the retarding potential device (region R) and neutral fragments formed in the F1 region as well.

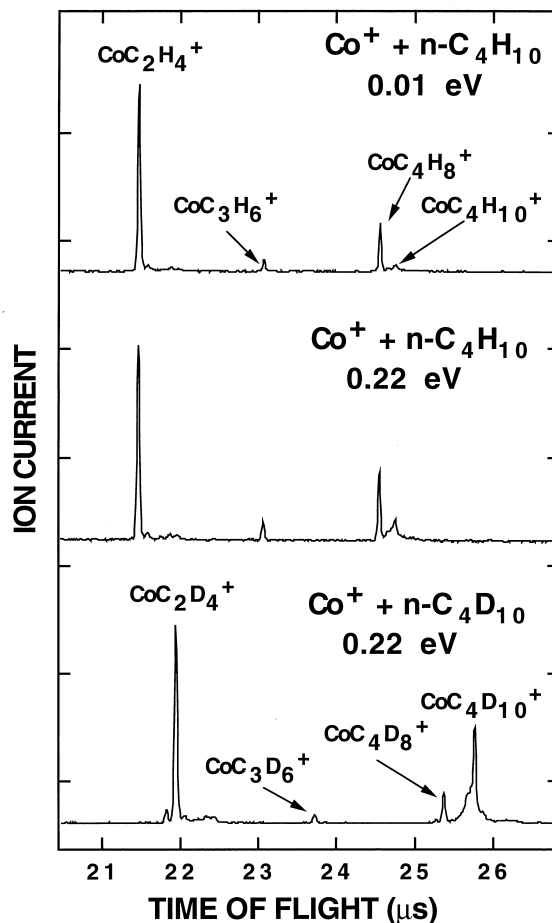


Fig. 1. Time-of-flight mass spectra of product region following collision of  $\text{Co}^+ + n\text{-C}_4\text{H}_{10}$  with ion extraction time  $t_{\text{ext}} = 8 \mu\text{s}$  and collision energy  $E_i = 0.01 \text{ eV}$  (top panel) and  $E_i = 0.22 \text{ eV}$  (middle panel). The bottom panel shows time-of-flight mass spectra of the product region for  $\text{Co}^+ + n\text{-C}_4\text{D}_{10}$  with ion extraction time  $t_{\text{ext}} = 8 \mu\text{s}$  and  $E_i = 0.22 \text{ eV}$ .

## 3. Results

### 3.1. $\text{Co}^+ + n\text{-butane}$ at $E_i = 0.01$ and $0.22 \text{ eV}$

In Fig. 1, we show product time-of-flight mass spectra recorded at collision energy  $E_i = 0.01$  and  $0.22 \text{ eV}$  collision energy with  $t_{\text{ext}} = 8 \mu\text{s}$ . At both collision energies, we find the absolute reaction cross section is  $(30 \pm 15)\%$  of the Langevin collision cross section. At  $0.01 \text{ eV}$  and  $t_{\text{ext}} = 8 \mu\text{s}$ , the dominant product (72%) is the  $\text{C}_2\text{H}_6$  elimination product,

Table 1  
Branching fractions for  $\text{Co}^+ + n\text{-butane}$  including complexes,  
 $t = 2\text{--}10 \mu\text{s}$  after collision<sup>a</sup>

$E_t$ (eV) <sup>b</sup>	$\text{CoC}_2\text{H}_4^+$	$\text{CoC}_3\text{H}_6^+$	$\text{CoC}_4\text{H}_8^+$	$\text{CoC}_4\text{H}_{10}^+$
0.01	$72 \pm 3$	$5 \pm 1$	$18 \pm 1$	$5 \pm 2$
0.22	$60 \pm 1$	$5 \pm 1$	$19 \pm 1$	$16 \pm 1$

<sup>a</sup> Data for  $t_{\text{ext}} = 8 \mu\text{s}$  and ion extraction energy 1280 eV, which places the time since initiation of  $\text{Co}^+ + n\text{-butane}$  in the range 2–10  $\mu\text{s}$ .

<sup>b</sup> Collision energy.

$\text{CoC}_2\text{H}_4^+$  [Eq. (1b)]. We also see 5% of the  $\text{CH}_4$  elimination product  $\text{CoC}_3\text{H}_6^+$  [Eq. (1c)], 18% of the  $\text{H}_2$  elimination product  $\text{CoC}_4\text{H}_8^+$  [Eq. (1d)] and 5% of the long-lived complex,  $\text{CoC}_4\text{H}_{10}^+$  [Eq. (1a)]. At  $E_t = 0.22 \text{ eV}$  and  $t_{\text{ext}} = 8 \mu\text{s}$ , we observe the same product ions but a slightly larger proportion of the complex. The branching fractions are 60%  $\text{CoC}_2\text{H}_4^+$  (+  $\text{C}_2\text{H}_6$ ), 5%  $\text{CoC}_3\text{H}_6^+$  (+  $\text{CH}_4$ ), 19%  $\text{CoC}_4\text{H}_8^+$  (+  $\text{H}_2$ ), and 16%  $\text{CoC}_4\text{H}_{10}^+$ . The ratio  $\text{CoC}_2\text{H}_4^+ : \text{CoC}_4\text{H}_8^+$  is constant for  $0.5 \leq t_{\text{ext}} \leq 8 \mu\text{s}$ . The ratio of  $\text{CoC}_2\text{H}_4^+ : \text{CoC}_3\text{H}_6^+ : \text{CoC}_4\text{H}_8^+$  intensity remains roughly constant with collision energy; the production of  $\text{CoC}_2\text{H}_4^+$  (+ $\text{C}_2\text{H}_6$ ) decreases slightly at the higher collision energy. Also, in the mass spectra taken at both the higher and the lower collision energies, the  $\text{CoC}_4\text{H}_{10}^+$  complex peaks appear rather broad relative to the narrow elimination product peaks. This is due to metastable decay of complexes in the drift region of the mass spectrometer and the subsequent slight separation of the parents and fragments in time due to the strong electric field at the detector. As described below, a retarding field placed near the end of the drift

Table 3  
Branching fractions for  $\text{Co}^+ + n\text{-butane-d}_{10}$  including complexes,  $t = 2\text{--}10 \mu\text{s}$  after collision<sup>a</sup>

$E_t$ (eV) <sup>b</sup>	$\text{CoC}_2\text{D}_4^+$	$\text{CoC}_3\text{D}_6^+$	$\text{CoC}_4\text{D}_8^+$	$\text{CoC}_4\text{D}_{10}^+$
0.22	$45 \pm 2$	$2 \pm 1$	$8 \pm 1$	$45 \pm 2$

<sup>a</sup> Data for  $t_{\text{ext}} = 8 \mu\text{s}$  and ion extraction energy 1280 eV, which places the time since initiation of  $\text{Co}^+ + n\text{-butane-d}_{10}$  in the range 2–10  $\mu\text{s}$ .

<sup>b</sup> Collision energy.

region will separate these fragment and parent ions in time.

The simple time-of-flight mass spectrum with  $t_{\text{ext}} = 8 \mu\text{s}$  (Fig. 1) in effect samples the decay kinetics of collision complexes over a uniform distribution of times in the window  $t = 2\text{--}10 \mu\text{s}$  since the initiation of a collision, as explained in detail previously [18]. The resulting “prompt” product branching fractions including adducts are summarized in Tables 1 and 3. In Tables 2 and 4, we compare the branching between the three elimination products under our conditions with that observed in earlier work. The branching between the three elimination channels is fairly insensitive to differences in collision energy and perhaps in electronic state distribution of  $\text{Co}^+$  among the different experiments.

The peaks from the three elimination products are comparably narrow for large extraction times. However, at 0.22 eV with  $t_{\text{ext}} = 0.8 \mu\text{s}$ , the  $\text{CoC}_2\text{H}_4^+$  (+ $\text{C}_2\text{H}_6$ ) peak clearly exhibits a tail toward longer times (Fig. 2), the characteristic signature of metastable complex decay in the extraction region of the mass spectrometer. The ions in the tail accelerate initially

Table 2  
Comparison of elimination product branching fractions for the reaction of  $\text{Co}^+ + n\text{-butane}$

$E_t$ (eV)	Technique <sup>a</sup>	$\text{CoC}_2\text{H}_4^+ + \text{C}_2\text{H}_6$	$\text{CoC}_3\text{H}_6^+ + \text{CH}_4$	$\text{CoC}_4\text{H}_8^+ + \text{H}_2$	Ref.
0.01	CB	76	5	19	This work
0.22	CB	71	6	23	This work
~0.5	IB + G	59	12	29	15
~1.0	IB + G	59	12	29	17
TE <sup>b</sup>	TMS	65	<1	35	16
TE <sup>b</sup>	CID	54	14	32	16

<sup>a</sup> CB: crossed beams; IB + G: ion beam + gas cell; TMS: tandem mass spectrometry; CID: collision induced dissociation.

<sup>b</sup> Thermal energy distributions near 300 K.

Table 4

Comparison of elimination product branching fractions for the reaction of  $\text{Co}^+ + n\text{-butane-}d_{10}$ 

$E_i$ (eV) <sup>a</sup>	Technique <sup>b</sup>	$\text{CoC}_2\text{D}_4^+ + \text{C}_2\text{D}_6$	$\text{CoC}_3\text{D}_6^+ + \text{CD}_4$	$\text{CoC}_4\text{D}_8^+ + \text{D}_2$	Ref.
0.22	CB	82	4	14	This work
TE	CID	71	12	17	[13]

<sup>a</sup> Collision energy.<sup>b</sup> CB: crossed beams.

as adduct ions  $\text{CoC}_4\text{H}_{10}^+$  fragment during extraction, and complete their acceleration as lighter  $\text{CoC}_2\text{H}_4^+$  elimination products. A single-exponential decay with  $330 \pm 100$  ns lifetime provides a sensible simultaneous fit of both the narrow component and the tail of the  $\text{CoC}_2\text{H}_4^+$  peak. At 0.01 eV the fitted lifetime (not shown) is very similar,  $350 \pm 100$  ns. We would also expect to be able to extract a decay lifetime from the  $\text{CoC}_3\text{H}_6^+ (+\text{CH}_4)$  peak. However,  $\text{CH}_4$  elimination is a very minor channel in this reaction, precluding a lifetime measurement even at the higher collision

energy. Since the extent of tailing due to metastable decay is strongly dependent on the mass difference between the fragment and the parent, we were also not able to observe tailing on the  $\text{CoC}_4\text{H}_8^+ (+\text{H}_2)$  peak.

The fraction of long-lived  $\text{CoC}_4\text{H}_{10}^+$  complexes observed in this work at  $t_{\text{ext}} = 8 \mu\text{s}$  is 5% at 0.01 eV and 16% at 0.22 eV. Within experimental error, these results do not change when the Ar backing pressure is doubled or halved or when the reagent backing pressure is varied over the range 20–120 Torr. Nor was any  $\text{Co}(n\text{-butane})_2^+$  observed. Thus we believe these are bimolecular collision complexes that have *not* been stabilized by a third-body collision. The average lifetime of the complexes can increase with increasing  $E_i$  because larger collision energy brings larger angular momenta to the complexes, which increases the effective barrier height for elimination channels and slows the overall decay rate [2–4].

The metastable decay of the long-lived  $\text{CoC}_4\text{H}_{10}^+$  complexes was probed with the retarding potential method. For  $t_{\text{ext}} = 8 \mu\text{s}$ , mass spectra such as those in Fig. 3 in effect sample the decay kinetics of collision complexes over a uniform distribution of times in the window  $t = 6\text{--}24 \mu\text{s}$  since initiation of a collision, as explained in detail earlier [18]. We report delayed fragmentation results only qualitatively here because of the small fraction of adduct ion in the  $\text{Co}^+ + n\text{-butane}$  reaction. For an ion extraction energy of 1280 eV, retarding potentials  $V_r > 400$  V can separate the  $\text{CoC}_4\text{H}_{10}^+$  peak into very long-lived adducts (lifetime  $> 25 \mu\text{s}$ ) and metastable fragmentation channels. At 0.22 eV, the most abundant delayed fragmentation products are  $\text{Co}^+ (+\text{C}_4\text{H}_{10})$  and  $\text{CoC}_2\text{H}_4^+ (+\text{C}_2\text{H}_6)$  that arise from decay in the F1 region.

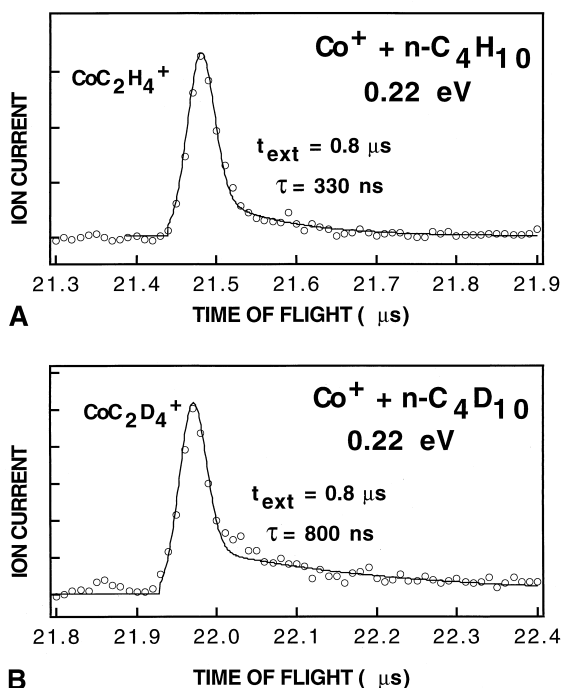


Fig. 2. Expanded view of ethane elimination product peak for  $E_i = 0.22$  eV with  $t_{\text{ext}} = 0.8 \mu\text{s}$  (dots): (a)  $\text{CoC}_4\text{H}_{10}^+$  complex decay fitted with  $1/e$  time constant of 330 ns, (b)  $\text{CoC}_4\text{D}_{10}^+$  complex decay fitted with time constant of 800 ns.

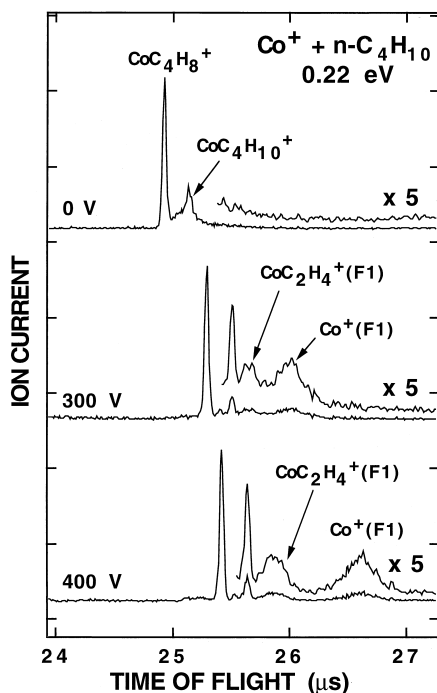


Fig. 3. Retarding field measurements for  $\text{Co}^+ + n\text{-C}_4\text{H}_{10}$  at  $E_t = 0.22$  eV and  $t_{\text{ext}} = 8$   $\mu\text{s}$ . The broad  $\text{CoC}_4\text{H}_{10}^+$  peak in the top trace (retarding voltage  $V_r = 0$ ) is separated for  $V_r = 300$  and  $400$  V into a sharp peak plus fragment peaks as indicated. See text for details.

### 3.2. $\text{Co}^+ + n\text{-butane-}d_{10}$ at $E_t = 0.22$ eV

For fixed  $E_t$ , the average lifetime of  $\text{Co}$  (*n*-butane)<sup>+</sup> complexes increases substantially upon deuteration (Fig. 1). At 0.23 eV, the fraction of adducts in the simple mass spectrum increases from 16% for  $\text{Co}^+ + n\text{-C}_4\text{H}_{10}$  to 45% for  $\text{Co}^+ + n\text{-C}_4\text{D}_{10}$ . The tail (Fig. 2) observed on the  $\text{CoC}_2\text{D}_4^+$  (+  $\text{C}_2\text{D}_6$ ) peak at shorter  $t_{\text{ext}}$  is now reasonably fit with a  $800 \pm 100$  ns lifetime, compared with the lifetime of  $330 \pm 100$  ns measured for the  $\text{CoC}_2\text{H}_4^+$  (+  $\text{C}_2\text{H}_6$ ) peak. The prompt product branching fractions ( $t = 2\text{--}10$   $\mu\text{s}$ ) for perdeuterated *n*-butane with  $t_{\text{ext}} = 8$   $\mu\text{s}$  are reported in Table 3. For *n*-butane- $d_{10}$  at 0.22 eV,  $\text{C}_2\text{D}_6$  elimination is favored 5:1 over  $\text{D}_2$  elimination; for comparison, for *n*-butane- $h_{10}$  at 0.22 eV,  $\text{C}_2\text{H}_6$  elimination is favored 3:1 over  $\text{H}_2$  elimination. The fraction of  $\text{CD}_4$  or  $\text{CH}_4$  elimination remains relatively constant.

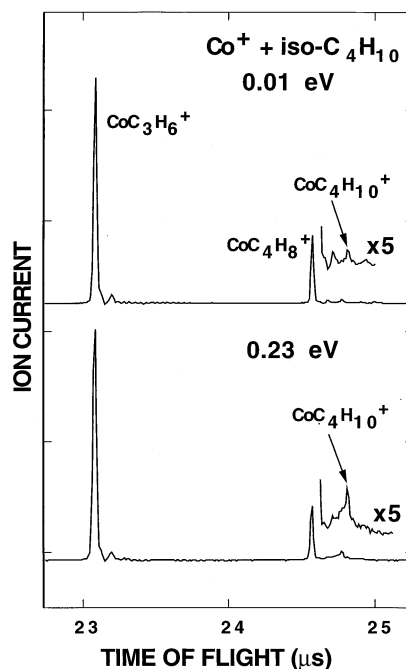


Fig. 4. Time-of-flight mass spectra of product region following collision of  $\text{Co}^+ + \text{iso-C}_4\text{H}_{10}$  with ion extraction time  $t_{\text{ext}} = 8$   $\mu\text{s}$  and collision energy  $E_t = 0.01$  eV (top panel) and  $E_t = 0.23$  eV (bottom panel).

### 3.3. $\text{Co}^+ + \text{isobutane}$ at $E_t = 0.01$ and $0.23$ eV

As shown in Fig. 4, at collision energy  $E_t = 0.01$  eV and  $t_{\text{ext}} = 8$   $\mu\text{s}$ , the dominant product (77%) is the  $\text{CH}_4$  elimination product  $\text{CoC}_3\text{H}_6^+$  [Eq. (2b)]. Also observed is 19%  $\text{H}_2$  elimination product  $\text{CoC}_4\text{H}_8^+$  [Eq. (2c)] and 3% long-lived complex  $\text{CoC}_4\text{H}_{10}^+$  [Eq. (2a)]. At the higher collision energy with  $t_{\text{ext}} = 8$   $\mu\text{s}$ , the branching fractions are 78%  $\text{CoC}_3\text{H}_6^+$  (+  $\text{CH}_4$ ), 16%  $\text{CoC}_4\text{H}_8^+$  (+  $\text{H}_2$ ), and 6%  $\text{CoC}_4\text{H}_{10}^+$ . The ratio of  $\text{CoC}_3\text{H}_6^+$ : $\text{CoC}_4\text{H}_8^+$  intensity remains roughly constant with collision energy and  $t_{\text{ext}}$ ; the production of  $\text{CoC}_4\text{H}_8^+$  (+  $\text{H}_2$ ) increases slightly at the higher collision energy (Table 5). In Table 6, we compare the branching between the two elimination products under our conditions with that observed in earlier work. Evidently differences in collision energy and/or electronic state distribution among the different experiments have only a minimal effect on the branching between  $\text{CH}_4$  and  $\text{H}_2$  elimination channels.

Table 5  
Branching fractions from  $\text{Co}^+$  + isobutane over time window  
 $t = 2\text{--}10 \mu\text{s}$  after initiation of collision<sup>a</sup>

$E_i$ (eV) <sup>b</sup>	$\text{CoC}_3\text{H}_6^+ + \text{CH}_4$	$\text{CoC}_4\text{H}_8^+ + \text{H}_2$	$\text{CoC}_4\text{H}_{10}^+$
0.01	$77 \pm 0.6$	$19 \pm 0.4$	$3.1 \pm 0.6$
0.23	$78 \pm 1.0$	$16 \pm 0.2$	$6.4 \pm 1.0$

<sup>a</sup> Data for  $t_{\text{ext}} = 8 \mu\text{s}$  and ion extraction energy 1280 eV, which places the time since initiation of  $\text{Co}^+$  + isobutane in the range of 2–10  $\mu\text{s}$ .

<sup>b</sup> Collision energy.

At very short  $t_{\text{ext}}$ , a tail toward longer times is observed on the  $\text{CoC}_3\text{H}_6^+$  peak (Fig. 5) because of metastable decay  $\text{CoC}_4\text{H}_{10}^+$  complexes in the extraction region of the mass spectrometer. At 0.23 eV, a single-exponential decay model with a  $270 \pm 100$  ns lifetime fits both the narrow component and the tail of the  $\text{CoC}_3\text{H}_6^+$  peak. At 0.01 eV the fitted lifetime (not shown) increases slightly to  $300 \pm 100$  ns.

At  $t_{\text{ext}} = 8 \mu\text{s}$ , the fraction of  $\text{CoC}_4\text{H}_{10}^+$  complexes from isobutane is 6% at 0.23 eV and 3% at 0.01 eV. Within experimental error, the proportion of long-lived complexes we observe does not vary with change in Ar backing pressure or reagent backing pressure. In addition, the formation of  $\text{Co}(\text{isobutane})_2^+$  was not detected. This evidence indicates our experiment runs within the single collision regime; the long-lived  $\text{CoC}_4\text{H}_{10}^+$  complexes have not been collisionally stabilized.

The application of a retarding potential late in the drift region of our time-of-flight mass spectrometer allows us to study the metastable decay of the

Table 6  
Comparison of elimination product branching fractions for reactions of  $\text{Co}^+$  + isobutane

$E_i$ (eV)	Technique <sup>a</sup>	$\text{CoC}_3\text{H}_6^+ + \text{CH}_4$	$\text{CoC}_4\text{H}_8^+ + \text{H}_2$	Ref.
0.01	CB	80	20	This work
0.23	CB	83	17	This work
~0.5	IB + G	73	27	15
~1.0	IB + G	77	23	17
TE <sup>b</sup>	TMS	50	48	16
TE <sup>b</sup>	CID	63	37	16

<sup>a</sup> CB: crossed beams; IB + G: ion beam + gas cell; TMS: tandem mass spectrometry; CID: collision induced dissociation.

<sup>b</sup> Thermal energy distributions near 300 K.

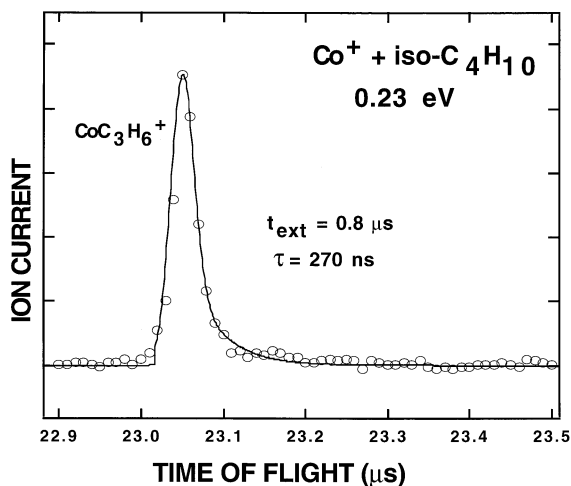


Fig. 5. Expanded view of  $\text{CoC}_2\text{H}_4^+$  (+  $\text{C}_2\text{H}_6$ ) product for  $E_i = 0.23$  eV with  $t_{\text{ext}} = 8 \mu\text{s}$  (dots). Solid line is fit to single exponential model of  $\text{CoC}_4\text{H}_{10}^+$  complex decay with  $1/e$  time constant of 270 ns.

long-lived  $\text{CoC}_4\text{H}_{10}^+$  complexes. Due to the small fraction of adduct ion in the  $\text{Co}^+$  + isobutane reaction, we again report these delayed fragmentation results only qualitatively. Retarding potentials  $V_r > 400$  V can separate the  $\text{CoC}_4\text{H}_{10}^+$  peak into very long-lived adducts (lifetime  $> 25 \mu\text{s}$ ) and metastable fragmentation channels. At 0.23 eV the most abundant delayed fragmentation products are  $\text{Co}^+$  (+  $\text{C}_4\text{H}_{10}$ ) and  $\text{CoC}_3\text{H}_6^+$  (+  $\text{CH}_4$ ) that arise from decay in the F1 region.

#### 4. Discussion

The reactions of  $\text{Co}^+$  + *n*-butane and  $\text{Co}^+$  + isobutane have been studied by a multitude of mass spectrometric techniques, as is apparent from a glance at Tables 2, 4, and 6. Despite this wealth of experimental information, including kinetic energy release distributions [16], isotopic labeling studies [15,16], reaction cross sections [15,17,27], and now time-resolved branching fractions, the detailed mechanisms of these reactions remain uncertain. Lacking electronic structure calculations, we will rely on ideas from theoretical studies on similar systems [2–4] to

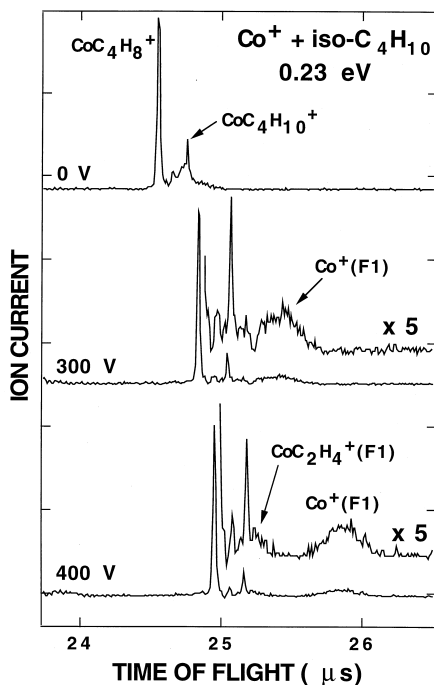


Fig. 6. Retarding field measurements for  $\text{Co}^+ + \text{iso-C}_4\text{H}_{10}$  at  $E_r = 0.23 \text{ eV}$  and  $t_{\text{ext}} = 8 \mu\text{s}$ . The broad  $\text{CoC}_4\text{H}_{10}^+$  peak in the top trace (retarding voltage  $V_r = 0$ ) is separated for  $V_r = 300$  and  $400 \text{ V}$  into a sharp peak plus fragment peaks as indicated. See text for details.

understand the pathways by which these reactions occur.

We have recently studied the related  $\text{Ni}^+ + \text{propane}$  [2],  $\text{Ni}^+ + n\text{-butane}$  [3], and  $\text{Co}^+ + \text{propane}$  [4] reactions in which we compared experimental results to the predictions of statistical rate modeling based on geometries and vibrational frequencies of key intermediates and transition states calculated using density functional theory (B3LYP). As a result of these studies and others [28–30], several unifying themes have emerged for reactions of  $\text{Co}^+$  and  $\text{Ni}^+$  with alkanes: (1) CC and CH insertions are energetically facile; branching between elimination pathways is determined by MCTSs. This contrasts with the stepwise elimination pathways proposed earlier [16]. The reason seems to be that  $d^7s$  and  $d^8s$  configurations of these metals lack enough empty and half-empty orbitals to form stable intermediates such as

$\text{M}(\text{H})_2(\text{alkene})^+$ , which are postulated energy minima in the stepwise mechanisms. (2) As a rough guide, the relative energies of the various MCTSs correlate with the strengths of the bonds into which the metal initially inserts:  $\text{CC} \ll \text{secondary CH} \ll \text{primary CH}$  [3]. The quality of *agostic interactions* between CH bonds of  $\beta$ -methyl groups and the metal atom in the MCTS seems important also [4–7]. (3) Only  $\beta$ -hydrogen migrations to the metal atom are feasible at low energy;  $\beta$ -alkyl shifts occur over very high barriers and should not contribute significantly at low collision energies. (4) Conservation of angular momentum plays an important role in determining the range of overall complex decay rates, as well as the product branching. Our goal in this discussion is to learn to what extent we can apply these themes to the reactions of  $\text{Co}^+ + n\text{-butane}$  and  $\text{Co}^+ + \text{isobutane}$  to obtain a good qualitative understanding of the elimination pathways.

#### 4.1. $\text{Co}^+ + n\text{-butane}$

The similarity of the experimental results for the reactions  $\text{Co}^+ + n\text{-butane}$  and  $\text{Ni}^+ + n\text{-butane}$  suggests they share a common mechanism. Both ions react at low energies to yield the same three  $\text{C}_2\text{H}_6$ ,  $\text{CH}_4$ , and  $\text{H}_2$  elimination products. For prompt fragmentation ( $< 10 \mu\text{s}$ ) at  $0.2 \text{ eV}$ , the branching ratios are 67:1:32 for  $\text{Ni}^+$  and 71:6:23 for  $\text{Co}^+$ . Both metals nearly skip over the  $\text{CH}_4$  channel and strongly favor  $\text{C}_2\text{H}_6$  over  $\text{H}_2$  elimination. Less than 20% adduct is observed in either reaction. Additionally, there is experimental evidence from collision induced dissociation (CID) work [12] for the existence of a bis(ethylene) intermediate in both the  $\text{Co}^+ + n\text{-butane}$  and  $\text{Ni}^+ + n\text{-butane}$  reactions. One subtle difference is that 10% of a  $\text{Co}(\text{butene})^+$  product is observed in CID studies of the reaction of  $\text{Co}^+ + n\text{-butane}$ , whereas in  $\text{Ni}^+ + n\text{-butane}$  only the bis(ethylene) intermediate is found [12]. As in  $\text{Ni}^+ + n\text{-butane}$ , the apparent nonexponential decay kinetics observed for  $\text{Co}^+ + n\text{-butane}$  indicates that angular momentum conservation is again important in determining the outcome of the reaction [3].

In contrast, the two metals differ substantially in

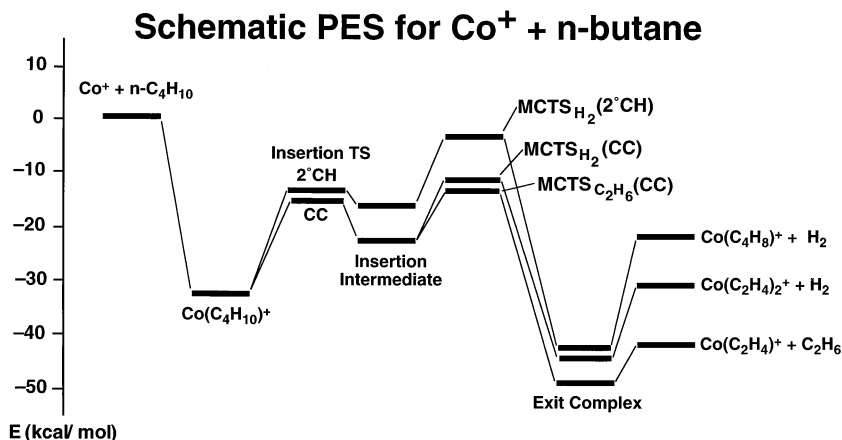


Fig. 7. Schematic reaction pathways for the  $\text{Co}^+ + n\text{-butane}$  reaction; probable low energy pathways to  $\text{CoC}_2\text{H}_4^+ + \text{C}_2\text{H}_6$  and  $\text{CoC}_4\text{H}_8^+ + \text{H}_2$  elimination products are shown. Energetics based on pathways from B3LYP calculations for  $\text{Ni}^+ + n\text{-butane}$ .

their reactions with propane. The ratio of  $\text{H}_2:\text{CH}_4$  elimination is consistently  $\sim 1:5$  for  $\text{Ni}^+ + \text{C}_3\text{H}_8$ , whereas it reverses to about 3:1 for  $\text{Co}^+ + \text{C}_3\text{H}_8$ . This effect is explained qualitatively by B3LYP calculations [4] as we discuss below. It is striking that a similar reversal does not occur in comparing the seemingly analogous  $\text{H}_2:\text{C}_2\text{H}_6$  branching for the  $\text{Ni}^+ + n\text{-butane}$  and  $\text{Co}^+ + n\text{-butane}$  reactions.

We have B3LYP results and guidance from statistical rate modeling for  $\text{Ni}^+ + \text{propane}$  [2] and  $n\text{-butane}$  [3] and for  $\text{Co}^+ + \text{propane}$  [4], but not for  $\text{Co}^+ + n\text{-butane}$ . For both of the propane reactions at low collision energy, this work indicates that  $\text{CH}_4$  elimination comes entirely from CC insertion and subsequent  $\beta$ -hydrogen migration over  $\text{MCTS}_{\text{CH}_4}(\text{CC})$ .  $\text{H}_2$  elimination comes predominantly from secondary CH insertion and subsequent  $\beta$ -hydrogen migration over  $\text{MCTS}_{\text{H}_2}(2^\circ \text{CH})$ . In B3LYP calculations, the relative energies of these two MCTSs changes substantially from  $\text{Ni}^+$  to  $\text{Co}^+$  in the proper direction to explain the significant shift in  $\text{H}_2:\text{CH}_4$  branching described above.

According to B3LYP theory [3], in the  $\text{Ni}^+ + n\text{-butane}$  reaction at low energy the  $\text{C}_2\text{H}_6$  comes from *central* CC insertion and subsequent  $\beta$ -hydrogen migration over  $\text{MCTS}_{\text{C}_2\text{H}_6}(\text{CC})$ , a pathway analogous to the  $\text{CH}_4$  elimination pathway in the propane reactions. However, the  $\text{H}_2$  elimination comes not from

$\text{MCTS}_{\text{H}_2}(2^\circ \text{CH})$ , which would be analogous to the propane case, but again from central CC insertion followed by a novel *double- $\beta$ -hydrogen migration* over  $\text{MCTS}_{\text{H}_2}(\text{central CC})$ . The second lowest energy pathway to  $\text{H}_2$  elimination goes over  $\text{MCTS}_{\text{H}_2}(2^\circ \text{CH})$ .

We tentatively assume the reactions of  $\text{Ni}^+$  and  $\text{Co}^+$  with  $n\text{-butane}$  at low collision energy share the common mechanism shown in Fig. 7. The key MCTSs are depicted in Fig. 8, based on the  $\text{Ni}^+$  calculations [3]. Association of the  $\text{Co}^+$  ion and  $n\text{-butane}$  results in formation of an ion-induced-dipole complex, the initial deep well ( $\sim 35$  kcal/mol below reactants) on the potential energy surface. The dominant elimination products  $\text{C}_2\text{H}_6$  and  $\text{H}_2$  arise primarily from insertion into the (weakest) central CC bond. The lowest energy pathway to  $\text{CH}_4$  elimination (not shown) presumably begins with initial insertion into the terminal CC bond, the second weakest bond of  $n\text{-butane}$ . The next lowest energy pathway involves secondary CH insertion leading to  $\text{H}_2$  elimination over  $\text{MCTS}_{\text{H}_2}(2^\circ \text{CH})$ . MCTSs arising from *primary* CH bond insertion in  $\text{Ni}^+ + n\text{-butane}$  were found to be sufficiently high in energy to exclude any contribution of these pathways at low  $E_t$  [3], so we neglect them here. If this mechanism is correct, our modeling experience indicates that the MCTS energies in Fig. 7

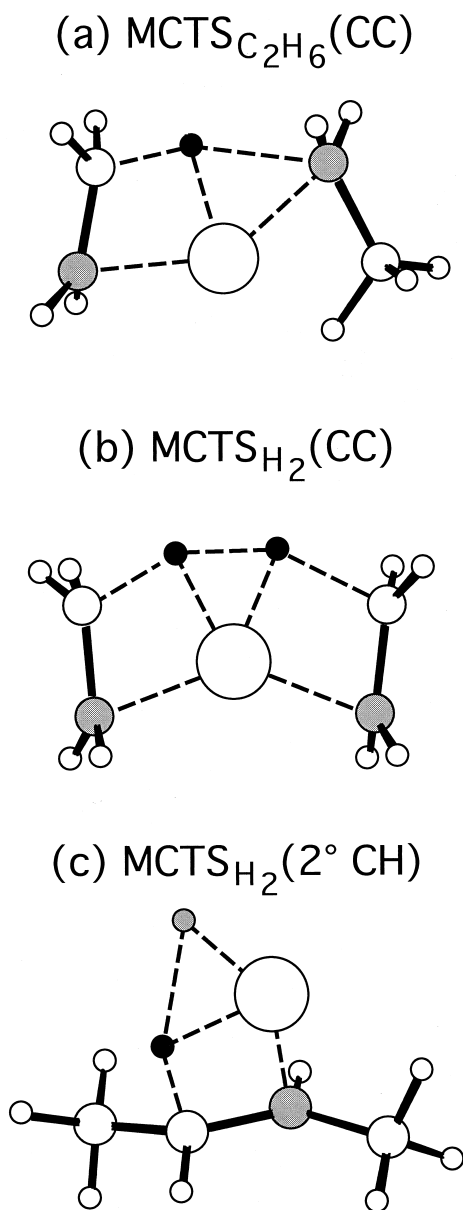


Fig. 8. Suggested structures for MCTSs on the lowest energy elimination pathways for  $\text{C}_2\text{H}_6$  and  $\text{H}_2$  elimination from  $\text{Co}^+ + n\text{-butane}$ , based on similar structures from B3LYP calculations for  $\text{Ni}^+ + n\text{-butane}$ . Shaded atoms formed the original bond into which  $\text{Co}^+$  inserted; black  $\beta$ -hydrogen atom(s) are migrating to make  $\text{C}_2\text{H}_6$  or  $\text{H}_2$ .

are placed to explain both the product branching and the overall cross section.

This picture explains the most important experimental observations nicely. The central CC insertion path dominates at low collision energy, producing all of the  $\text{C}_2\text{H}_6$  and most of the  $\text{H}_2$ . For the  $\text{CoC}_4\text{H}_8^+ + \text{H}_2$  channel, this is consistent with the observation from collision-induced dissociation that the  $\text{CoC}_4\text{H}_8^+$  fragments from decay of long-lived  $\text{CoC}_4\text{H}_{10}^+$  adducts consist of some 90%  $\text{Co}(\text{ethylene})_2^+$  [12]. Unlike in  $\text{Ni}^+ + n\text{-butane}$ , some 10% of a  $\text{Co}(\text{butene})^+$  product is also observed. It could be either  $\text{Co}(\text{1-butene})^+$  or  $\text{Co}(\text{2-butene})^+$ .  $\text{Co}(\text{2-butene})^+$  is exactly the product that would be formed by passage over  $\text{MCTS}_{\text{H}_2}(2^\circ \text{CH})$ , the second lowest barrier for  $\text{H}_2$  elimination in Fig. 7. We therefore place this barrier low enough so that it can contribute a fraction of the  $\text{H}_2$  at low collision energy. For  $\text{Ni}^+$ , B3LYP places  $\text{MCTS}_{\text{H}_2}(2^\circ \text{CH})$  relatively higher. Corroboration of this difference between  $\text{Co}^+$  and  $\text{Ni}^+$  comes from our study of the  $\text{Co}^+$  and  $\text{Ni}^+$  reactions with propane [2,4]. In those reactions, B3LYP finds a completely analogous lowering of  $\text{MCTS}_{\text{H}_2}(2^\circ \text{CH})$  by  $\sim 4$  kcal/mol in  $\text{Co}^+$  compared with  $\text{Ni}^+$  [4]. The suggested reason is the stronger stabilizing  $\beta$ -methyl agostic interactions available to  $\text{MCTS}_{\text{H}_2}(2^\circ \text{CH})$  in the case of  $\text{Co}^+$ , which has one more empty (electron acceptor) d-orbital than  $\text{Ni}^+$ . Geometric evidence for this effect is clear from the corresponding lengthening of a CH bond in the  $\beta$ -methyl group.

The same electronic effects should be present in the  $n\text{-butane}$  reactions, which neatly explains why  $\text{MCTS}_{\text{H}_2}(2^\circ \text{CH})$  can be competitive with the central CC insertion channels in  $\text{Co}^+ + n\text{-butane}$  but not in  $\text{Ni}^+ + n\text{-butane}$ . The dominant pathway at low collision energy remains central CC insertion, which produces all of the  $\text{C}_2\text{H}_6$  over  $\text{MCTS}_{\text{C}_2\text{H}_6}(\text{CC})$  and much of the  $\text{H}_2$  over  $\text{MCTS}_{\text{H}_2}(\text{central CC})$ . This may also begin to explain why there is only a small difference in the ratio  $\text{H}_2:\text{C}_2\text{H}_6$  between the  $\text{Ni}^+ + n\text{-butane}$  and  $\text{Co}^+ + n\text{-butane}$  reactions. As shown in Fig. 8, there are no  $\beta$ -methyl agostic interactions to be found in  $\text{MCTS}_{\text{H}_2}(\text{central CC})$ , but there is a  $\beta$ -methyl interaction in  $\text{MCTS}_{\text{C}_2\text{H}_6}(\text{CC})$ . According to this idea, in changing from  $\text{Ni}^+$  to  $\text{Co}^+$  those reactants that insert in the central CC bond should make a larger fraction of  $\text{C}_2\text{H}_6$  in preference over  $\text{H}_2$ , but this could

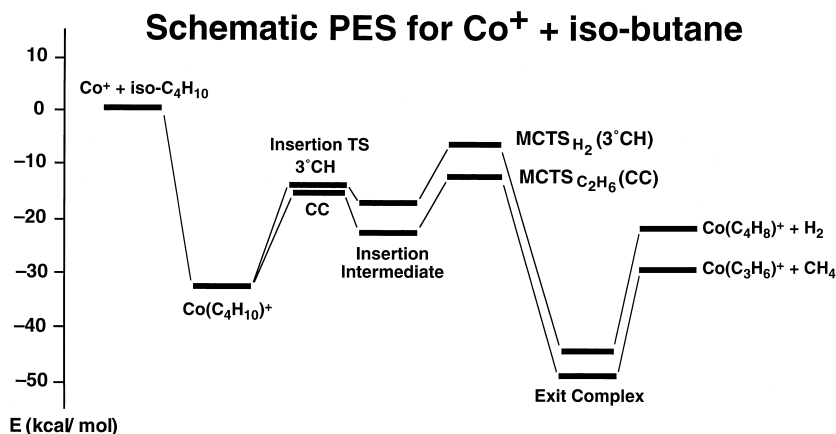


Fig. 9. Schematic reaction pathways for the  $\text{Co}^+$  + isobutane reaction; probable low energy pathways to  $\text{CoC}_3\text{H}_6^+ + \text{CH}_4$  and  $\text{CoC}_4\text{H}_8^+ + \text{H}_2$  elimination products are shown. Energetics based on pathways from B3LYP calculations for  $\text{Co}^+$  + propane.

be compensated by the introduction of a new source of  $\text{H}_2$  over  $\text{MCTS}_{\text{H}_2}(2^\circ \text{CH})$ . Quantitative tests of these ideas using B3LYP theory are highly desirable.

#### 4.2. $\text{Co}^+$ + isobutane

In order to apply mechanistic ideas from B3LYP theory to the reaction of  $\text{Co}^+$  + isobutane, we consider isobutane to be a “mutated” propane, i.e., a propane in which one of the secondary hydrogens has been replaced by a methyl group. This allows a qualitative comparison with  $\text{Co}^+$  + propane, a reaction for which B3LYP calculations of the key MCTSs are available. The reactions of  $\text{Co}^+$  with propane and  $\text{Co}^+$  with isobutane appear similar in that the only elimination products in both reactions are  $\text{CH}_4$  and  $\text{H}_2$ . However, the ratio of  $\text{CH}_4$ : $\text{H}_2$  elimination products at the higher collision energy is *reversed*, from 84:16 for isobutane to 26:74 for propane [4]. In addition, the fraction of adduct is less than 10% of the total products for isobutane, while it is 43% for propane. Thus, although we might expect the *structures* of key intermediates and transition states of the two reactions to be analogous, the *energetics* are likely somewhat different, and they will be adjusted from the  $\text{Co}^+$  + propane case to fit experimental observations as explained below.

Schematic reaction pathways for the two major

elimination products in the  $\text{Co}^+$  + isobutane reaction are shown in Fig. 9. Suggestions for the structures of the key MCTSs, based on B3LYP calculations for  $\text{Co}^+$ -propane [4] and the “mutated propane” idea are shown in Fig. 10. According to theory, for  $\text{Co}^+$  + propane the lowest energy pathway to  $\text{CH}_4$  elimination arises from initial insertion into a CC bond; the lowest energy pathway to  $\text{H}_2$  elimination involves initial insertion into a secondary CH bond. For  $\text{Co}^+$  + isobutane, the analogous low energy pathways are insertion into a CC bond leading to  $\text{CH}_4$  elimination, and insertion into a *tertiary* CH bond leading to  $\text{H}_2$  elimination. Beauchamp, Bowers, and co-workers [16] report 100% HD elimination for the  $\text{H}_2$  elimination channel for the reaction of  $\text{Co}^+$  with isobutane- $\text{d}_1$ . Two plausible mechanisms leading to this product involve initial primary CH insertion or initial tertiary CH insertion. Based on B3LYP results for both  $\text{Ni}^+$  and  $\text{Co}^+$  with propane [2,4], it is improbable that either  $\text{CH}_4$  or  $\text{H}_2$  elimination involves initial insertion into a *primary* CH bond, the strongest bond in isobutane. The bond dissociation energy for the primary CH bond in isobutane is 98 kcal/mol, while the tertiary CH bond strength is only 92 kcal/mol [31]. In addition, the MCTSs following initial secondary CH insertion in propane [2,4] and *n*-butane [3] are found to be 6–10 kcal/mol lower in energy than those involving primary CH insertion. An

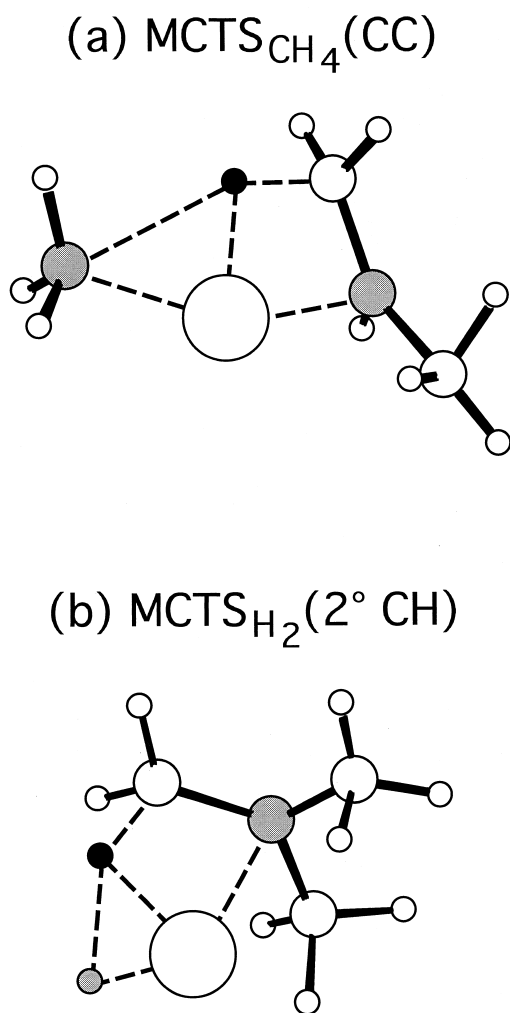


Fig. 10. Suggested structures for MCTSs on the lowest energy elimination pathways for (a)  $\text{CH}_4$  and (b)  $\text{H}_2$  elimination from  $\text{Co}^+$  + isobutane based on similar structures from B3LYP calculations for  $\text{Co}^+$  + propane. Shaded atoms formed the original bond into which  $\text{Co}^+$  inserted; black  $\beta$ -hydrogen atom is migrating to make  $\text{CH}_4$  or  $\text{H}_2$ .

initial tertiary insertion MCTS should lie even lower in energy relative to primary CH insertion. Thus, in keeping with the principles outlined above, we assert that  $\text{H}_2$  arises exclusively from tertiary CH insertion, in agreement with the pathway proposed earlier by Hanratty et al. [16].

Our placement of intermediates and transition states on the schematic  $\text{Co}^+$  + isobutane reaction

pathways of Fig. 9 is guided by both B3LYP results and experimental observations. For  $\text{Ni}^+$  +  $\text{C}_3\text{H}_8$  and  $n\text{-C}_4\text{H}_{10}$ , comparing B3LYP energetics with the thermochemistry of the bare alkane, we earlier noted (Fig. 13 of Ref. 3) a correlation between the relative strength of the bonds into which the metal initially inserts and the relative energetics of the corresponding insertion intermediates. Applying this idea to  $\text{Co}^+$  + isobutane, we can estimate the energy separation of the insertion intermediates for the two pathways. We place the insertion intermediates roughly at the same separation (6 kcal/mol) that was calculated between secondary CH bond and CC bond insertions in  $\text{Ni}^+$  +  $\text{C}_3\text{H}_8$  and  $n\text{-C}_4\text{H}_{10}$ , narrowing the gap slightly because  $\text{H}_2$  elimination from isobutane involves insertion into the weaker tertiary CH bond. We found less correlation between the height of the insertion *transition states* and the bond dissociation energies. CH insertion transition states seemed to be stabilized more than CC insertions, probably because of the greater directionality of the CC bond [32]. The nearly degenerate placement of the insertion transition states again reflects the smaller tertiary bond energy compared with the secondary CH bond involved in propane or  $n$ -butane reactions.

The energies of the MCTSs relative to reactants are likely similar to those in  $\text{Co}^+$  and  $\text{Ni}^+$  +  $n$ -butane (−6 to −10 kcal/mol), rather than very close to reactants as in  $\text{Co}^+$  and  $\text{Ni}^+$  with propane (−2 to −3 kcal/mol). This is apparent from the large proportion of elimination products relative to adducts, and from the experimental observation that the fraction of adducts *increases* with collision energy. This latter effect arose also in  $\text{Co}^+$  and  $\text{Ni}^+$  +  $n$ -butane. The modeling explained this as a result of angular momentum conservation in these reactions. The lowering of the  $\text{CH}_4$  and  $\text{H}_2$  elimination MCTSs in the  $\text{Co}^+$  + isobutane reaction relative to  $\text{Co}^+$  + propane is likely due to the weaker bonds being broken and to the new stabilizing agostic interactions made possible by the mutation of a secondary hydrogen to a methyl group. Depending on the rotation of this methyl group, one or two new  $\beta$ -hydrogen- $\text{Co}^+$  interactions are possible in  $\text{MCTS}_{\text{H}_2}(3^\circ \text{CH})$ , as suggested in Fig. 10.

Since we expect the relative heights of the multicenter transition states in the  $\text{Co}^+$  + isobutane reaction to determine the experimentally observed branching fractions, we place  $\text{MCTS}_{\text{CH}_4}$  below  $\text{MCTS}_{\text{H}_2}$  ( $3^\circ$  CH). As we have observed for propane and *n*-butane,  $\text{MCTS}_{\text{H}_2}$  ( $2^\circ$  CH) seems to be better stabilized by agostic interactions in reactions with  $\text{Co}^+$  than with  $\text{Ni}^+$ . This trend extends to isobutane as well, since the fraction of  $\text{H}_2$  to  $\text{CH}_4$  increases for  $\text{Ni}^+$  relative to  $\text{Co}^+$  according to branching fractions reported by several groups [15,16].

In summary, simple extensions of ideas based on B3LYP theory for other reactions can explain essentially all of the observations for  $\text{Co}^+$  + *n*-butane and  $\text{Co}^+$  + isobutane. If we are to extend these unifying themes to other new systems, the question arises as to the generality of multicenter transition states. Density functional theory calculations for  $\text{Co}^+$  + ethane [7],  $\text{Ni}^+$  + ethane [8],  $\text{Fe}^+$  + ethane [6], and  $\text{Fe}^+$  + propane [5] have found MCTSs to be the highest points on the potential energy surfaces for these reactions as well. By contrast, a recent experimental study of *second row* group 8 cations with alkanes postulates that no MCTSs are involved [29,31]. The authors argue that because of the decrease in atomic promotion energy from high-spin to low-spin  $d^{x-1}s$  states on moving from  $\text{Fe}^+$ ,  $\text{Co}^+$ , and  $\text{Ni}^+$  to  $\text{Ru}^+$ ,  $\text{Rh}^+$ , and  $\text{Pd}^+$ , MCTSs will not be needed in the 4d-series cations. It may be possible for the 4d ions to pair one additional electron spin and use the resulting unoccupied orbital to form covalently bound intermediates, as in the original stepwise mechanisms. Therefore, although there is strong testimony from theory to the importance of MCTSs in *first row* group 8 metal cation reactions with alkanes, it remains an open question whether or not MCTSs are important for other metal cations. More theory is needed.

## 5. Conclusion

We have reexamined the  $\text{Co}^+$  + *n*-butane and isobutane reactions under carefully controlled, crossed-beam conditions to measure the time evolution of the long-lived complexes. A simple extension

of the ideas derived from statistical modeling based on density functional theory calculations (B3LYP) for  $\text{Ni}^+$  + propane,  $\text{Ni}^+$  + *n*-butane, and  $\text{Co}^+$  + propane can readily explain our observations and other experiments as well. Our postulated reaction pathways are satisfyingly consistent with the low-lying pathways found by theory for related reactions.

## Acknowledgements

JCW thanks the National Science Foundation (CHE-9616724) and the Donors of the Petroleum Research Foundation (PRF-33441-AC6) for generous support of this research. SSY acknowledges support from a Lubrizol Fellowship.

## References

- [1] K. Eller, H. Schwarz, Chem. Rev. 91 (1991) 1121.
- [2] S.S. Yi, M.R.A. Blomberg, P.E.M. Siegbahn, J.C. Weisshaar, J. Phys. Chem. 102 (1998) 395.
- [3] M.R.A. Blomberg, P.E.M. Siegbahn, S.S. Yi, R.J. Noll, J.C. Weisshaar, J. Phys. Chem. A 103 (1999) 7254.
- [4] S.S. Yi, J.C. Weisshaar, M.C. Holthausen, W. Koch, J. Phys. Chem. A, work in progress.
- [5] M.C. Holthausen, W. Koch, Helv. Chim. Acta 79 (1996) 1939.
- [6] M.C. Holthausen, A. Fiedler, H. Schwarz, W. Koch, J. Phys. Chem. 100 (1996) 6236.
- [7] M.C. Holthausen, W. Koch, J. Am. Chem. Soc. 118 (1996) 9932.
- [8] M.R.A. Blomberg, P.E.M. Siegbahn, unpublished results.
- [9] A.D. Becke, J. Chem. Phys. 84 (1986) 4524.
- [10] M. Brookhart, M.L.H. Green, J. Organomet. Chem. 250 (1983) 395.
- [11] R.H. Grubbs, G.W. Coates, Acc. Chem. Res. 29 (1996) 85.
- [12] D.B. Jacobson, B.S. Freiser, J. Am. Chem. Soc. 105 (1983) 5197.
- [13] R.B. Freas, D.P. Ridge, J. Am. Chem. Soc. 102 (1980) 7129.
- [14] P.B. Armentrout, L.F. Halle, J.L. Beauchamp, J. Am. Chem. Soc. 103 (1981) 6501.
- [15] R. Houriet, L.F. Halle, J.L. Beauchamp, Organometallics 2 (1983) 1818.
- [16] M.A. Hanratty, J.L. Beauchamp, A.J. Illies, P.A.M. van Koppen, M.T. Bowers, J. Am. Chem. Soc. 110 (1988) 1.
- [17] P.B. Armentrout, J.L. Beauchamp, J. Am. Chem. Soc. 103 (1981) 784.
- [18] R.J. Noll, S.S. Yi, J.C. Weisshaar, J. Phys. Chem. 102 (1998) 386.

- [19] R.J. Noll, Doctoral Dissertation Thesis, University of Wisconsin-Madison, 1994.
- [20] M.D. Morse, J.B. Hopkins, P.R.R. Langridge-Smith, R.E. Smalley, *J. Chem. Phys.* 79 (1983) 5316.
- [21] D.E. Powers, S.G. Hansen, M.E. Geusic, A.C. Pulu, J.B. Hopkins, T.G. Dietz, M.A. Duncan, P.R.R. Langridge-Smith, R.E. Smalley, *J. Phys. Chem.* 86 (1982) 2556.
- [22] J. Sugar, C. Corliss, *J. Phys. Chem. Ref. Data* 14 (1985) 513 (suppl. 2).
- [23] R.H. Page, C.S. Gudeman, *J. Opt. Soc. Am. B7* (1990) 1761.
- [24] W.C. Wiley, I.H. McLaren, *Rev. Sci. Instrum.* 26 (1955) 1150.
- [25] R.J. Gallagher, Doctoral Dissertation Thesis, Yale University, 1972.
- [26] G. Cooper, Y. Zheng, G.R. Burton, C.E. Brion, *Rev. Sci. Instrum.* 64 (1993) 1140.
- [27] M.A. Hanratty, J.L. Beauchamp, A.J. Illies, M.T. Bowers, *J. Am. Chem. Soc.* 107 (1985) 1788.
- [28] C.L. Haynes, E.R. Fisher, P.B. Armentrout, *J. Phys. Chem.* 100 (1996) 18 300.
- [29] J.K. Perry, Thesis, California Institute of Technology, 1994.
- [30] P.A.M. van Koppen, M.T. Bowers, C. Haynes, P.B. Armentrout, *J. Am. Chem. Soc.* 120 (1998) 5704.
- [31] P.B. Armentrout, Y.-M. Chen, *J. Am. Soc. Mass Spectrom.* 10 (1999) 821.
- [32] P.A.M. van Koppen, J. Brodbelt-Lustig, M.T. Bowers, D.V. Dearden, J.L. Beauchamp, E.R. Fisher, P.B. Armentrout, *J. Am. Chem. Soc.* 113 (1991) 2359.